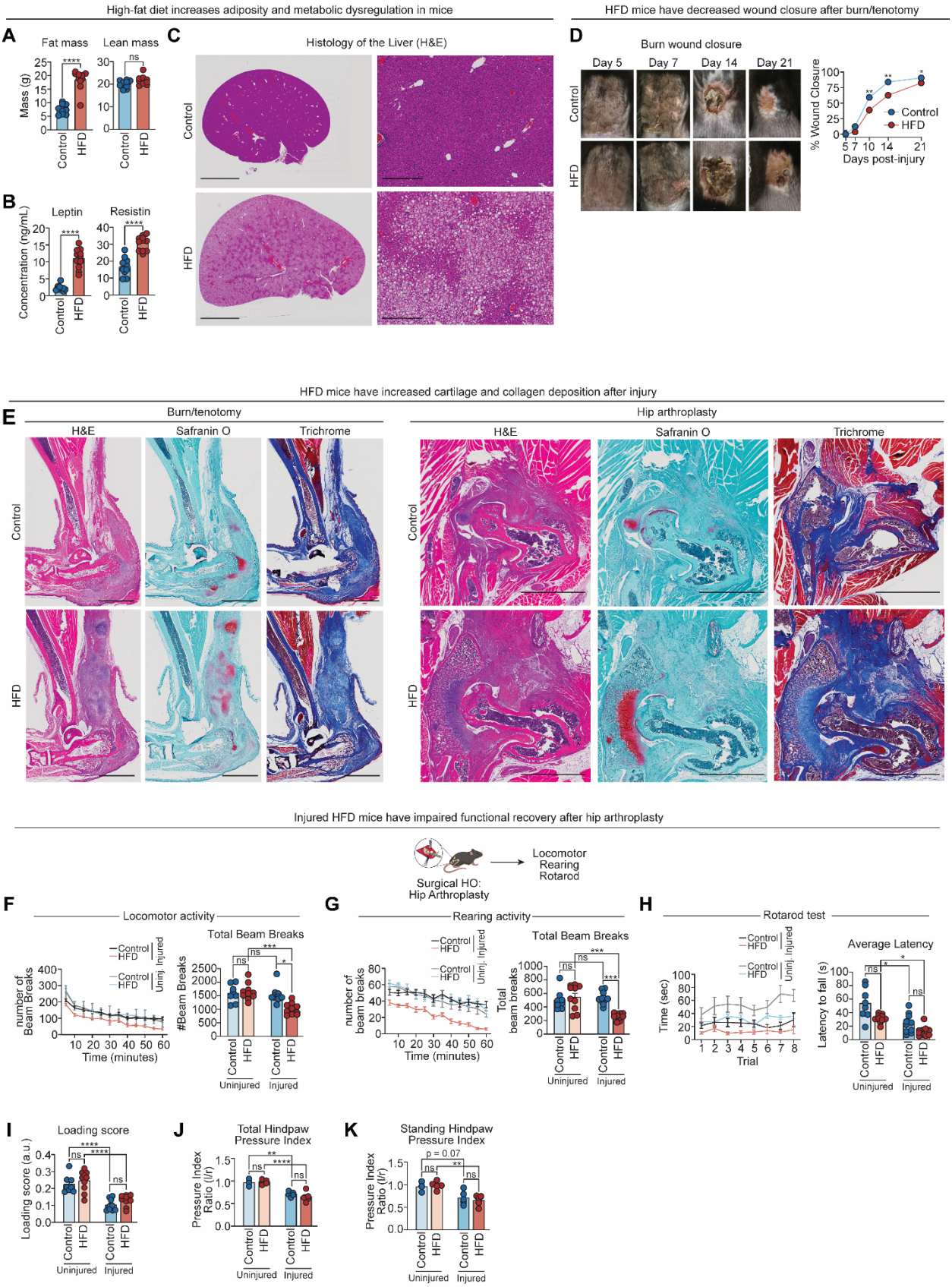
High-fat diet increases adiposity and metabolic dysregulation in mice
A
Fat mass
Lean mass
Mass (g)
Control
HFD
B
Leptin
Resistin
Concentration (ng/mL)
C
Histology of the Liver (H&E)
HFD mice have decreased wound closure after burn/tenotomy
D
Burn wound closure
Day 5
Day 7
Day 14
Day 21
% Wound Closure
Days post-injury
HFD mice have increased cartilage and collagen deposition after injury
E
Burn/tenotomy
Hip arthroplasty
H&E
Safranin O
Trichrome
Injured HFD mice have impaired functional recovery after hip arthroplasty
Surgical HO:
Hip Arthroplasty
Locomotor
Rearing
Rotarod
F
Locomotor activity
Total Beam Breaks
number of Beam Breaks
Time (minutes)
#Beam Breaks
Uninjured
Injured
G
Rearing activity
number of beam breaks
Total beam breaks
H
Rotarod test
Time (sec)
Trial
Average Latency
Latency to fall (s)
I
Loading score
Loading score (a.u.)
J
Total Hindpaw Pressure Index
Pressure Index Ratio (l/r)
K
Standing Hindpaw Pressure Index

Supplemental Figure 1: Metabolic and functional characterization of control and HFD mice pre- and post-injury.

(A) Fat mass and lean mass pre-injury measured with NMR in HFD and control mice (n = 10 mice/group).
(B) Serum leptin and resistin levels pre-injury (n = 10-11 mice/group).
(C) Representative liver H&E sections at 9 weeks post-B/T. Low- and high-magnification images are shown. Scale bars = 5mm (left), 500 μM (right).
(D) Time course of percentage of burn wound closure normalized to baseline wound area (n = 3 mice/ group).
(E) H&E, Safranin O, and Trichrome staining in the B/T (left panel) and HA (right panel) model at 3 weeks post-injury in HFD and control mice. Images demonstrate cartilage and collagen deposition in the injured limb or hip. Scale bars = 2.5 mm.
(F) Locomotor activities were measured as number of beam breaks in control and HFD mice with and without HA at 6 weeks post-HA. Left: time course of activity for the 4 groups. Right: total mean activity per mouse (n = 8-10 mice/group).
(G) Rearing activities were measured as number of beam breaks at 6 weeks post-HA. Left: time course of rearing for the 4 groups. Right: total mean rearing per mouse (n = 8-10 mice/group).
(H) Rotarod testing showing the latency to fall of the rod (sec) at 6 weeks post-HA. Left: time course of rotarod performance across 8 trials. Right: mean latency to fall per mouse (n = 8-10 mice/group).
(I) Hindlimb loading score as a proxy for mechanical load (n = 8-10 mice/group).
(J) Total hindpaw pressure index (left/right hindpaw) (n = 3-5 mice/group).
(K) Standing hindpaw pressure index (left/right hindpaw) (n = 3-5 mice/group).

HO, heterotopic ossification; B/T, burn/tenotomy; HA, Hip Arthroplasty; HFD, high-fat diet; NMR; nuclear magnetic resonance; μCT, micro-computed tomography; Hematoxylin and eosin, H&E. Means ± SEM are plotted. All experiments are representative of at least two independent experiments. Statistics: Mann-Whitney (A, B), two-tailed Student's t test (D), Kruskal-Wallis (F, H), or one-way ANOVA (G, I, J, K). *$p < 0.05$; **$p < 0.01$; ***$p < 0.001$; ****$p < 0.0001$; ns, not significant.

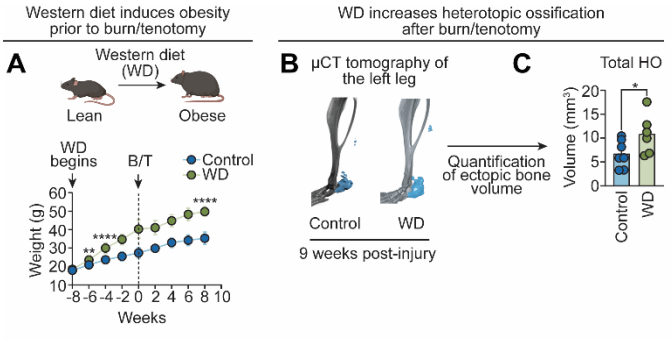

Supplemental Figure 2: Western diet promotes HO.
(A) Weights of Western diet (WD) and control mice after diet initiation. Mice were started on the WD 8 weeks prior to undergoing B/T and were followed for 9 weeks (n = 8-10 mice/group).
(B) Representative μCT images of ankle HO in the injured leg of WD and control mice 9 weeks after B/T.
(C) μCT quantification of total HO volume at 9 weeks post-injury (n = 6-7 mice/group).
HO, heterotopic ossification; WD, Western Diet; B/T, burn/tenotomy; μCT, micro-computed tomography. Means ± SEM are plotted. All experiments are representative of at least two independent experiments. Statistics: two-tailed Student's t test (A) or Mann-Whitney (C). *$p < 0.05$; **$p < 0.01$; ****$p < 0.0001$.

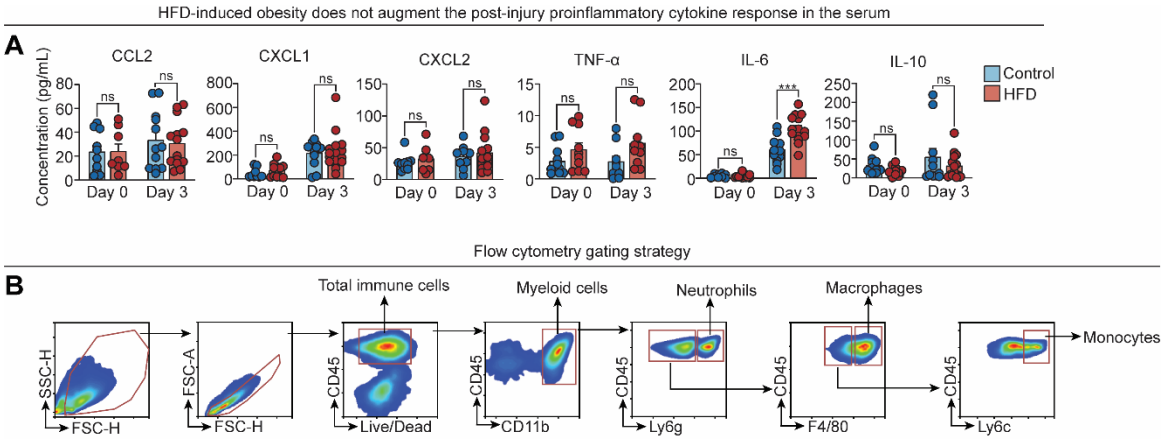

Supplemental Figure 3: Serum cytokine profiling and flow cytometry gating strategy for HO-site immune cells.

(A) Serum CCL2, CXCL1, CXCL2, TNFα, IL-6, and IL-10 (day 0 and day 3 post-B/T) in HFD and control mice. Cytokine levels were compared between dietary conditions at each time point (day 0 or day 3 post-B/T) (n = 9-10 mice/group).

(B) Gating strategy for identifying immune populations in the injury site. Cell subsets include total immune cells (live $CD45^+$), neutrophils (live $CD45^+$ $CD11b^+Ly6g^+$), macrophages (live $CD45^+CD11b^+$ $Ly6g^-$ $F4/80^+$), and monocytes (live $CD45^+CD11b^+Ly6g^-F4/80^-Ly6c^+$).

HFD, high-fat diet; B/T, burn/tenotomy. Means ± SEM are plotted. All experiments are representative of at least two independent experiments. Statistics: Mann-Whitney test (A). ***$p < 0.001$; ns, not significant.

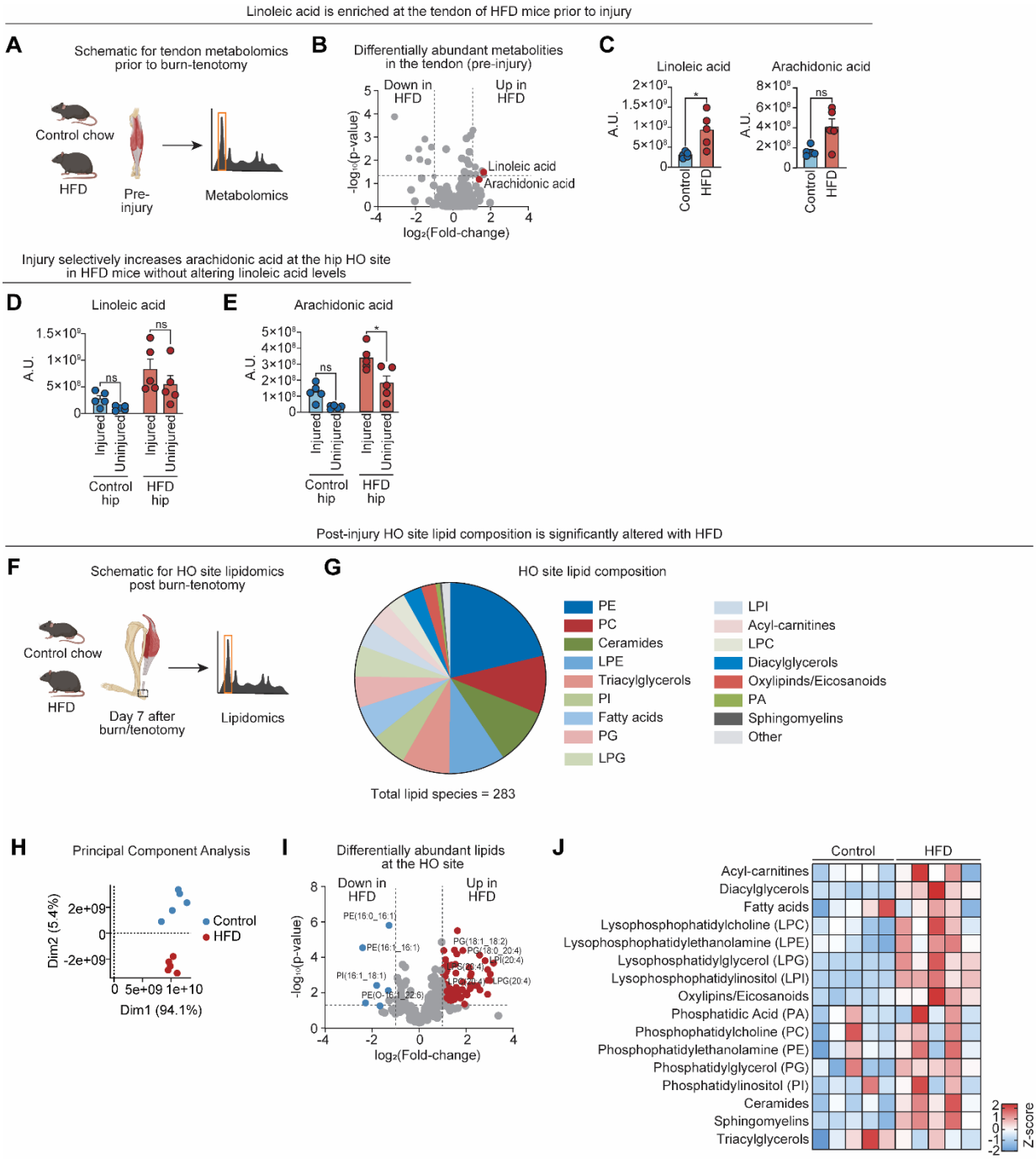

Supplemental Figure 4: Baseline tendon metabolomics and post-injury lipid alterations at the HO site.

(A) Experimental schematic of metabolomic characterization of uninjured tendons in HFD and control mice at day 0 before B/T.

(B) Volcano plot of uninjured tendon metabolites with LA and AA metabolites noted in red. The horizontal line indicates statistical significance ($p < 0.05$). The vertical lines denote $\log_2$FC = -1 and +1.

(C) Quantification of LA and AA abundance before B/T (n = 5 mice/group).

(D) Quantification of LA abundance in the injured and uninjured hips at day 7 post-HA; Metabolite levels were compared between injured and uninjured hips within each dietary condition (n = 5 mice/group). Data from Figure 3J were replotted to allow direct comparison with uninjured groups.
(E) Quantification of AA abundance in the injured and uninjured hips at day 7 post-HA; Metabolite levels were compared between injured and uninjured hips within each dietary condition (n = 5 mice/group). Data from Figure 3K were replotted to allow direct comparison with uninjured groups.
(F) Experimental schematic of lipidomic characterization of control and HFD HO sites at day 7 post-B/T.
(G) Pie chart showing the distribution of HO-site lipid classes in the dataset. Total lipid species = 283.
(H) PCA showing distinct lipid profiles in the HO site. PC1 and PC2 explain 94.1% and 5.4% of total variance respectively (n = 5 mice/group).
(I) Volcano plot of HFD vs. control HO-site lipids. The horizontal line indicates statistical significance ($p < 0.05$). The vertical lines denote $\log_2FC = -1$ and +1. Red dots (up in HFD) signify lipids which have $p < 0.05$ and $\log_2FC > 1$ and blue dots (down in HFD) signify lipids which have $p < 0.05$ and $\log_2FC < -1$. Top lipids in HFD contain AA-acyl chains: LPG 20:4, LPS 20:4, LPI 20:4, LPG 20:4.
(J) Heatmap of HO-site lipid classes. Values are normalized as z-scores (n = 5 mice/group).
B/T, burn/tenotomy; HFD, high-fat diet; LA, linoleic acid; AA, arachidonic acid; HA, hip arthroplasty; PCA; Principal component analysis; FC, Fold-change. Means ± SEM are plotted. All experiments are representative of at least two independent experiments. Statistics: Mann-Whitney test (C) and one-way ANOVA (D, E). *$p < 0.05$; ns, not significant.

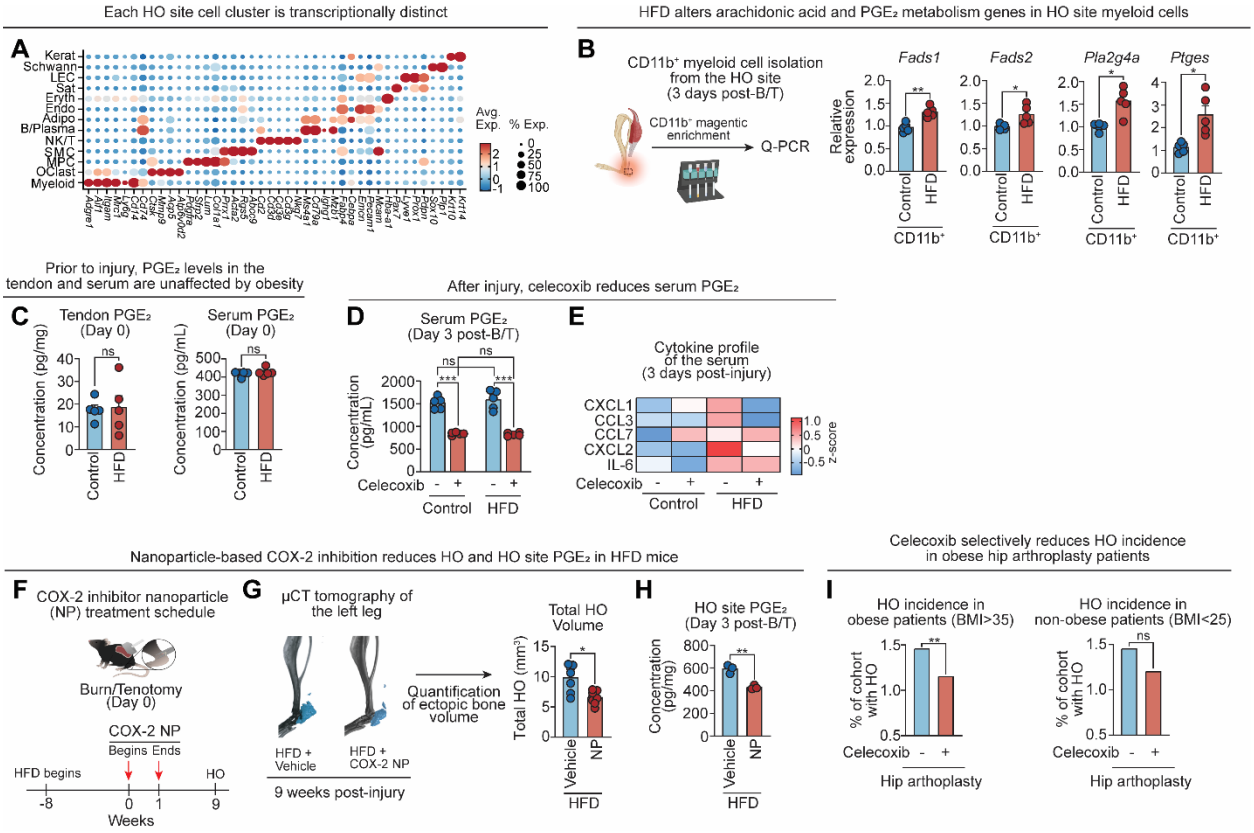

Supplemental Figure 5: Myeloid COX-2 drives PGE_2 production at the HO site, which is suppressed by COX-2 inhibition.

(A) Dot plot of canonical marker genes in each cluster from the scRNA-seq data obtained from control and HFD HO sites pre- and post-injury. Unbiased clustering categorized cells into the following cell types: B/plasma cells (n = 18,051 cells), myeloid cells (n = 64,110 cells), endothelial cells (n = 21,625 cells), mesenchymal progenitor cells (n = 46,547 cells), NK/T cells (n = 3,768 cells), satellite cells (n = 1,987 cells), smooth muscle cells (n = 8,475 cells), lymphatic endothelial cells (n = 1,207 cells), Schwann cells (n = 2,185 cells), adipocytes (n = 718 cells), erythrocytes (n = 581 cells), osteoclasts (n = 4,981 cells), and keratinocytes (n = 8,104 cells).

(B) Left: Schematic of $CD11b^+$ myeloid cell magnetic enrichment in control and HFD HO sites at day 3 post-B/T. Right: Bar graphs show the relative expression of genes related to LA/AA and PGE_2 metabolism (*Fads1, Fads2, Pla2g4a, and Ptges*) in $CD11b^+$ HO-site myeloid cells measured via qPCR (n = 5 mice/group).

(C) Quantification of tendon and serum PGE_2 at day 0 post-B/T. Tendon values are normalized to total protein (n = 5 mice/group).

(D) Quantification of serum PGE_2 in control, control + celecoxib, HFD, and HFD + celecoxib groups at day 3 post-B/T (n = 5 mice/group). Control and HFD values from Figure 4D are replotted to allow direct comparison with celecoxib-treated groups.

(E) Serum cytokines in control, control + celecoxib, HFD, and HFD + celecoxib mice at day 3 post-B/T. Values are normalized as z-scores (n = 4-5 mice/group).

(F) COX-2 inhibitor nanoparticle (COX-2 NP) treatment schedule. Dextran or dextran-conjugated COX-2 inhibitor-loaded nanoparticles were injected subcutaneously near the injury site daily for 1-week post-B/T in HFD mice.

(G) Representative µCT images of HO (left) and µCT quantification of total HO volume (right) at the ankle joint in each group (HFD + vehicle and HFD + COX-2 NP) at 9 weeks post- B/T (n = 7-8 mice/group).

(H) HO-site PGE_2 levels in HFD + vehicle and HFD + COX-2 NP-treated mice at day 3 post-B/T. Values are normalized to total protein (n = 3 mice/group).
(I) Incidence of HO in obese patients after hip arthroplasty treated with or without celecoxib (Left) and non-obese patients treated with or without celecoxib (Right) for 1-month post-surgery. (Left: n = 24,915 patients/cohort; Right: n = 11,191 patients/cohort).
HO, heterotopic ossification; B/T, burn/tenotomy; LA, linoleic acid; AA, arachidonic acid; COX, Cyclooxygenase; PGE_2, prostaglandin E_2; UMAP, uniform manifold approximation and projection; scRNA-seq, single-cell RNA-sequencing; NP, nanoparticle. Means ± SEM are plotted. All experiments are representative of at least two independent experiments. Statistics: Mann-Whitney (B, C, G), one-way ANOVA (D), two-tailed Student's t test (H), or Chi-Square (I). $*p < 0.05$; $**p < 0.01$; $****p < 0.0001$; ns, not significant.

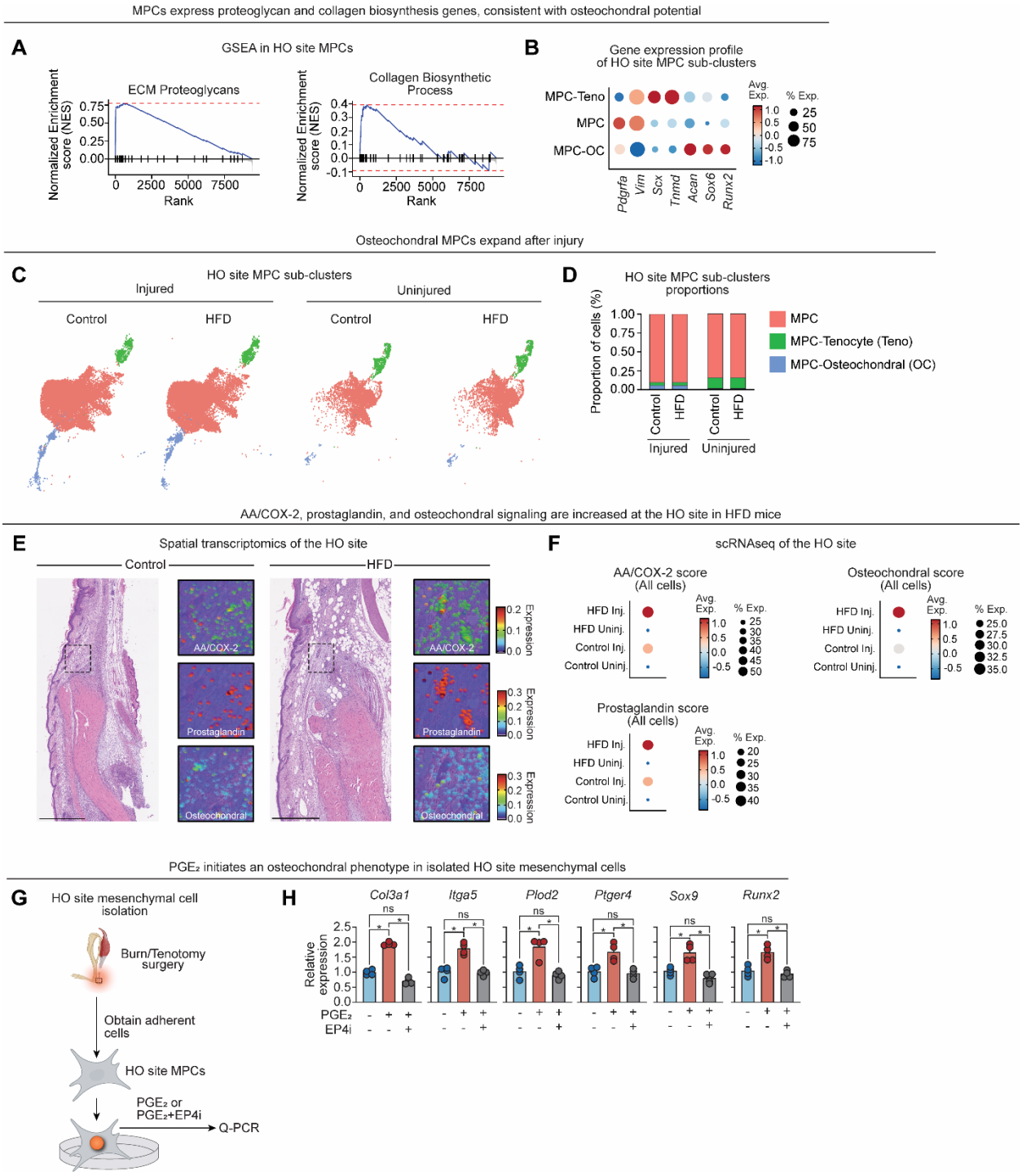

Supplemental Figure 6: HFD-induced obesity and COX-2 signaling promote extracellular matrix and osteochondral gene programs at the HO site.

(A) Gene set enrichment analysis (GSEA) using normalized enrichment scores (NES) of HFD vs. control MPCs. NES shows upregulation of ECM-proteoglycans and collagen biosynthesis in HFD MPCs relative to control MPCs after injury; Collagen Biosynthesis NES = 1.853, $p = 6.59 \times 10^{-3}$; ECM Proteoglycans NES = 3.361, $p = 1.019 \times 10^{-12}$.

(B) Gene expression profiles of the 3 HO site MPC subclusters (MPC-Teno, MPC-OC, and undifferentiated MPCs) defined by marker gene expression pre- and post-injury.
(C) UMAP of MPC subclusters, including MPC-Tenocytes (MPC-Teno) and MPC-Osteochondral cells (MPC-OC) split by injury status and diet.
(D) HO-site MPC sub-cluster proportions split by injury status and diet.
(E) Representative HD spatial gene expression of AA/COX-2-related, prostaglandin synthesis, and osteochondral differentiation genes within the HO-forming region at the distal end of the Achilles tendon 7 days post-injury. Each dot represents a cell with the color indicating its relative gene expression. (AA/COX-2-related genes: *Ptgs2*, *Ptger2*, *Ptger4*, *Fads1*, *Fads2*, *Ptges*, *Pla2g4a*, *Elovl2*, *Elovl5;* Prostaglandin synthesis genes*: Ptgs1, Ptgs2, Ptges;* Osteochondral differentiation genes: *Acan, Sox9, Ibsp, Col2a1, Bmp2, Bmp7, Runx2, Pdgfra*). Scale bar = 1mm.
(F) HO-site scRNA-seq analysis of corresponding gene module expression (AA/COX-2, prostaglandin synthesis, and osteochondral differentiation) from all cells pre- and post-injury in HFD and control mice.
(G) Schematic of MPC isolation and treatment with PGE_2. MPCs were isolated 7 days after B/T and treated with either PGE_2, PGE_2 + EP4 inhibitor (L-161,982), or vehicle for 24 hours, and subsequently collected for qPCR analysis.
(H) qPCR analysis of MPC osteochondral-related genes (*Col3a1, Itga5, Plod2, Ptger4, Sox9, Runx2*) treated with PGE_2, PGE_2 + EP4 inhibitor, or vehicle for 24 hours; n = 5 mice per group.
UMAP, uniform manifold approximation and projection; scRNA-seq, single-cell RNA-sequencing; MPC, mesenchymal progenitor cell; AA, arachidonic acid; COX-2, cyclooxygenase 2; PGE_2, prostaglandin E_2; EP4, Prostaglandin E_2 receptor 4. Means ± SEM are plotted. Statistics: one-way ANOVA (H). *$p < 0.05$; ns, not significant.

Diet Name	**Control**		**HFD**		**WD**		**Low-LA HFD**	
Label	gm	kcal	gm	kcal	gm	kcal	gm	kcal
Protein	19.0	20.0	26.2	20.0	24.0	20.0	26.0	20.0
Carbohydrate	67.0	70.0	26.3	20.0	41.0	35.0	26.0	20.0
Fat	4.0	10.0	34.9	60.0	24.0	45.0	35.0	60.0
Total		100.0		100.0		100.0		100.0
kcal/gm	3.8		5.2		4.7		5.2	
Ingredients	**Control**		**HFD**		**WD**		**Low-LA HFD**	
Added Cholesterol (mg)	0.0	0.0	0.0	0.0	242.2	0.0	0.0	0.0
Beef Tallow	0.0	0.0	0.0	0.0	0.0	0.0	135.0	1215.0
Calcium Carbonate	5.5	0.0	5.5	0.0	5.5	0.0	5.5	0.0
Casein	0.0	0.0	200.0	800.0	200.0	800.0	200.0	800.0
Casein, 30 Mesh	200.0	800.0	0.0	0.0	0.0	0.0	0.0	0.0
Cellulose	0.0	0.0	0.0	0.0	50.0	0.0	0.0	0.0
Cellulose, BW200	0.0	0.0	50.0	0.0	0.0	0.0	50.0	0.0
Cholesterol	0.0	0.0	0.0	0.0	0.1	0.0	0.0	0.0
Cholesterol (mg/kg)	0.0	0.0	0.0	0.0	282.2	0.0	0.0	0.0
Choline Bitartrate	2.0	0.0	2.0	0.0	2.0	0.0	2.0	0.0
Coconut Oil	0.0	0.0	0.0	0.0	0.0	0.0	0.0	0.0
Coconut Oil, 101	0.0	0.0	0.0	0.0	0.0	0.0	0.0	0.0
Corn Starch	506.2	2024.8	0.0	0.0	0.0	0.0	0.0	0.0
DiCalcium Phosphate	13.0	0.0	13.0	0.0	13.0	0.0	13.0	0.0
FD&C Blue Dye #1	0.0	0.0	0.1	0.0	0.0	0.0	0.0	0.0
FD&C Red Dye #40	0.0	0.0	0.0	0.0	0.0	0.0	0.0	0.0
FD&C Yellow Dye #5	0.0	0.0	0.0	0.0	0.1	0.0	0.0	0.0
L-Cystine	3.0	12.0	3.0	12.0	3.0	12.0	3.0	12.0
Lard	20.0	180.0	245.0	2205.0	177.5	1598.0	0.0	0.0
Maltodextrin 10	125.0	500.0	125.0	500.0	0.0	0.0	125.0	500.0
Menhaden Oil	0.0	0.0	0.0	0.0	0.0	0.0	0.0	0.0
Mineral Mix S10026	10.0	0.0	0.0	0.0	10.0	0.0	10.0	0.0
Mineral Mix, S10026	0.0	0.0	10.0	0.0	0.0	0.0	0.0	0.0
Olive Oil	0.0	0.0	0.0	0.0	0.0	0.0	54.0	486.0
Palm Oil	0.0	0.0	0.0	0.0	0.0	0.0	81.0	729.0
Potassium Citrate, 1 H2O	16.5	0.0	16.5	0.0	16.5	0.0	16.5	0.0
Safflower Oil	0.0	0.0	0.0	0.0	0.0	0.0	0.0	0.0
Soybean Oil	25.0	225.0	25.0	225.0	25.0	225.0	0.0	0.0
Sucrose	68.8	275.2	68.8	275.0	345.6	1382.0	68.8	275.0
Vitamin Mix V10001	10.0	40.0	10.0	40.0	10.0	40.0	10.0	40.0
Total	1055.05	4057.0	773.9	4057.0	858.223	4057.0	773.8	4057.0

Supplemental Table 1: Dietary Ingredients. Diet composition (grams) and caloric content (kcal) of rodent high-fat and control diets included in the study. HFD, high-fat diet; WD, Western diet; Low-LA HFD, low linoleic acid high-fat diet.

Rank	Pathway	Impact	Scaled p-value	Sum
1	Linoleic acid metabolism	1.00	0.64	1.64
2	Taurine and hypotaurine metabolism	0.60	0.85	1.45
3	Arachidonic acid metabolism	0.30	0.89	1.19
4	Ascorbate and aldarate metabolism	0.16	1.00	1.16
5	Phenylalanine and tyrosine metabolism	1.00	0.02	1.02

Supplemental Table 2: HO-site Metabolic Pathway Analysis. List of metabolic pathways elevated in HFD versus control HO sites, ranked by a composite score calculated as the sum of pathway impact (0-1) and scaled $-\log_{10}(p \text{ value})$ (p values were normalized to 0-1 range).

Fatty Acid Composition				
	Control	**HFD**	**WD**	**Low-LA**
ALA (g)	2.1	5.1	4.2	1.9
DHA (g)	0.0	0.0	0.0	0.0
EPA (g)	0.0	0.0	0.0	0.0
LA (g)	17.8	72.7	56.2	18.3
MUFA (% of total FA)	29.7	35.9	35.5	45.7
PUFA (% of total FA)	46.8	31.9	32.9	7.6
SFA (% of total FA)	23.5	32.2	31.6	43.5
Total MUFA (g)	12.8	91.2	67.7	122.0
Total PUFA (g)	20.2	81.0	62.8	20.4
Total SFA (g)	10.1	81.7	60.2	115.9
Total Fat (g)	43.1	253.9	190.7	258.3
kcal/g	3.8	5.2	4.7	5.2
ω-3 (g)	2.1	5.3	4.4	1.9
ω-6 (g)	17.9	73.7	57.0	18.4
ω-6/ω-3	8.4	13.9	13.1	9.8

Supplemental Table 3: Fatty Acid Composition of all Diets. Fatty acid composition (grams) of rodent high-fat and control diets included in the study. HFD, high-fat diet; WD, Western diet; Low-LA HFD, low linoleic acid high-fat diet; ALA, α linolenic acid; DHA, Docosahexaenoic acid; EPA, Eicosapentaenoic acid; LA, linoleic acid; SFA, Saturated fatty acids; MUFA, Monounsaturated fatty acids; PUFA, Polyunsaturated fatty acids; ω-3, omega-3; ω-6, omega-6.

Supplemental Video 1 (related to Fig. S1): BlackBox recording of injured control diet mouse post-hip arthroplasty. Representative video recording acquired from BlackBox from an injured control mouse 1 week following hip arthroplasty. This recording was used to calculate the total and standing hindpaw pressure index (left/right), which was quantified in Supplemental Figure 1, J-K.

Supplemental Video 2 (related to Fig. S1): BlackBox recording of injured HFD mouse post-hip arthroplasty. Representative video recording acquired from BlackBox from an injured HFD mouse 1 week following hip arthroplasty. This recording was used to calculate the total and standing hindpaw pressure index (left/right), which was quantified in Supplemental Figure 1, J-K.

Supplemental Video 3 (related to Fig. S1): BlackBox recording of uninjured control diet mouse. Representative video recording acquired from BlackBox from an uninjured control mouse. This recording was used to calculate the total and standing hindpaw pressure index (left/right), which was quantified in Supplemental Figure 1, J-K.

Supplemental Video 4 (related to Fig. S1): BlackBox recording of uninjured HFD diet mouse. Representative video recording acquired from BlackBox from an uninjured HFD mouse. This recording was used to calculate the total and standing hindpaw pressure index (left/right), which was quantified in Supplemental Figure 1, J-K.